Intratumoral Heterogeneity of Tumor Infiltration of Glioblastoma Revealed by Joint Histogram Analysis of Diffusion Tensor Imaging

Chao Li, MD[1,2], Shuo Wang, Bsc[3], Jiun-Lin Yan, MD[1,4,5], Rory J. Piper, MRCS[1], Hongxiang Liu, PhD FRCPath[6], Turid Torheim, PhD[7,8], Hyunjin Kim, PhD[7], Natalie R. Boonzaier, PhD[1,9], Rohitashwa Sinha, MRCS[1], Tomasz Matys, MD PhD[3,10], Florian Markowetz, PhD[7,8], and Stephen J. Price, PhD FRCS[1,11]

Corresponding author: Chao Li

Email: cl647@cam.ac.uk

1Cambridge Brain Tumor Imaging Laboratory, Division of Neurosurgery, Department of Clinical Neurosciences, University of Cambridge, Addenbrooke's Hospital, Cambridge, UK;

[2]Department of Neurosurgery, Shanghai General Hospital, Shanghai, China;

[3]Department of Radiology, University of Cambridge, Cambridge, UK;

[4]Department of Neurosurgery, Chang Gung Memorial Hospital, Keelung, Taiwan;

[5]Chang Gung University College of Medicine, Taoyuan, Taiwan;

[6]Molecular Malignancy Laboratory, Hematology and Oncology Diagnostic Service, Addenbrooke's Hospital, Cambridge, UK.

[7]Cancer Research UK Cambridge Institute, University of Cambridge, Cambridge, UK;

[8]CRUK & EPSRC Cancer Imaging Centre in Cambridge and Manchester, Cambridge, UK;

[9]Developmental Imaging and Biophysics Section, Institute of Child Health, University College London, London, UK

[10]Cancer Trials Unit Department of Oncology, Addenbrooke's Hospital, Cambridge, UK;

[11]Wolfson Brain Imaging Centre, Department of Clinical Neurosciences, University of Cambridge, Cambridge, UK;

Running title: Joint histogram analysis of diffusion tensor imaging

Funding

This study was funded by a National Institute for Health Research (NIHR) Clinician Scientist Fellowship (SJP, project reference NIHR/CS/009/011); CRUK core grant C14303/A17197 and A19274 (FM lab); Cambridge Trust and China Scholarship Council (CL & SW); the Chang Gung Medical Foundation and Chang Gung Memorial Hospital, Keelung, Taiwan (JLY); CRUK & EPSRC Cancer Imaging Centre in Cambridge & Manchester (FM & TT, grant C197/A16465); Royal College of Surgeons of England (RS); NIHR Cambridge Biomedical Research Centre (TM & SJP). The Human Research Tissue Bank is supported by the NIHR Cambridge Biomedical Research Centre. We would like to acknowledge the support of National Institute for Health Research, the University of Cambridge, Cancer Research UK and Hutchison Whampoa Limited. The views expressed are those of the author(s) and not necessarily those of the NHS, the NIHR or the Department of Health.

Conflict of Interest: none

Total word count: 6436

Manuscript type: Original research

Advances in knowledge

1. Joint histogram analysis of the isotropic (p) and anisotropic (q) components of the diffusion tensor imaging can reflect the intratumoral heterogeneity of glioblastoma infiltration.
2. Incremental prognostic values for the prediction of overall survival and progression-free survival can be achieved by the joint histogram features, when integrated with IDH-1 mutation, MGMT methylation status and other clinical factors.
3. The non-enhancing tumor subregion in which water molecules display decreased isotropic movement and increased anisotropic movement are potentially representative of a more invasive tumor habitat.

Implications for patient care

This study helps us to understand how the infiltrative patterns of glioblastoma contribute to patient outcomes. The invasive subregion identified by this approach may have clinical implications for personalized surgical resection and targeted radiation therapy.

Summary Statement

Although diffusion tensor imaging has been accepted as a sensitive method in depicting white matter disruption, the difficulty in interpreting high-dimensional tensor may hinder its further clinical application. Joint histogram analysis of the decomposed components of tensor imaging is proposed as a potential solution for this challenge, and a reference to other imaging analysis using multiple biomarkers.

Abstract

Purpose

To solve the challenge of interpreting diffusion tensor imaging (DTI), we proposed a joint histogram analysis of the isotropic (p) and anisotropic (q) components of DTI. We explored the heterogeneity of glioblastoma infiltration using the joint histogram features and evaluated their prognostic values.

Materials and methods

A total of 115 primary glioblastoma patients were prospectively recruited and preoperatively imaged. Patients underwent maximal safe resection. DTI was processed and decomposed into p and q components. Pixel values were extracted from DTI-p and -q maps and used to construct the univariate and joint histograms, in contrast-enhancing and non-enhancing regions respectively. Eight joint histogram features were obtained and then correlated with patient survival and tumor progression rate. Their prognostic values were examined and compared with clinical factors using receiver operating characteristic curves.

Results

Both univariate and joint histogram showed that the subregion of increased DTI-p and decreased DTI-q accounted for the largest proportion. However, additional diffusion patterns can be identified via joint histogram analysis. Particularly, a higher proportion of decreased DTI-p and increased DTI-q in non-enhancing region contributed to worse progression-free survival and worse overall survival (both HR = 1.12, $p < 0.001$); the proportion of this subregion showed a positive correlation ($p = 0.010$, $r = 0.35$) with tumor progression rate.

Conclusion

Joint histogram analysis of DTI can provide a comprehensive measure of heterogeneity in infiltration and prognostic values for glioblastoma patients. The subregion of decreased DTI-p and increased DTI-q in non-enhancing region may indicate a more invasive habitat.

Key words

Glioblastoma; Magnetic Resonance Imaging; Diffusion Tensor Imaging; Heterogeneity.

Introduction

Glioblastoma is the commonest primary malignant tumor in the central nervous system of adults (1). It is among the most lethal cancers, characterized by diffuse infiltration into the normal brain tissue (2), which renders a total resection impossible. Progression after surgery is almost inevitable, and predominantly manifest adjacent to the resection cavity (3).

It is recognized that glioblastoma is heterogeneous in its infiltrative pattern. Some tumors may disseminate into the surrounding brain tissue earlier and more intensively (4). Recent genomic findings have revealed that multiple tumor clones co-exist in the same tumor and may display diverse biological traits (5, 6). Migratory tumor clones may contribute to a more diffuse and invasive phenotype, which is thought to be especially responsible for treatment failure (3). Therefore, understanding the intratumoral heterogeneity of glioblastoma infiltration is of clinical significance for targeted surgery and radiotherapy.

Magnetic resonance imaging (MRI) has unique advantages in understanding spatial variations within glioblastoma. Current clinical management is primarily based on structural sequences, among which the contrast enhancement on post-contrast T1-weighted imaging is most widely used. However, these findings are limited since it just reflects the failure of blood brain barrier. Other sequences, such as fluid attenuated inversion recovery (FLAIR), although have been combined in patient assessment (7), but still proved to be non-specific in detecting tumor infiltration (8).

Diffusion tensor imaging (DTI), a method that measures the magnitude and direction of the movement of water molecules, has shown its sensitivity in detecting tumor infiltration (9). Glioblastoma is recognized to preferentially migrate along the white matter tracts and causes disruption to the microstructure of the white matter tracts (10). The diffusion of water molecules in the tumor core and peritumoral brain tissue is consequently altered. By decomposing the tensor into isotropic (DTI-p) and anisotropic (DTI-q) components, the directional diffusion of water molecules can be measured (11). This approach has been identified to be useful in predicting tumor progression (4) and patient survival (12). However, it remains to be discovered if integrating these decomposed components can offer a more comprehensive measure of tumor infiltration. Furthermore, several molecular biomarkers, such as isocitrate dehydrogenase (IDH) mutations (13) and oxygen 6–methylguanine-DNA methyltransferase (MGMT) promoter methylation (14) have been reported to be of diagnostic and prognostic significance for glioblastoma. Whether these DTI markers, particularly DTI-p and -q, can provide additional value to molecular markers is still unclear.

In this study, we sought to propose a novel DTI interpretation method by using the joint histogram analysis of DTI-p and -q. With this method we explored the heterogeneity of tumor infiltration and examined the prognostic value of tumor infiltrative patterns for patient survival. Our hypothesis was that the joint histogram analysis of DTI-p and -q would provide: 1) a more comprehensive measure of heterogeneity of tumor infiltration; 2) a more accurate detection of infiltrative subregions which are more responsible for tumor progression; and 3) incremental

prognostic values for glioblastoma patients when integrated with IDH-1 mutation, MGMT methylation status and other clinical factors.

Methods

Patient population

This study was approved by the local institutional review board. Signed informed consent was obtained from all patients. Patients with supratentorial primary glioblastoma were prospectively recruited for surgical resection from July 2010 to August 2015. All patients displayed good performance status (World Health Organization performance status 0-1). Exclusion criteria included history of a previous brain tumor, cranial surgery, radiotherapy/chemotherapy, or contraindication for MRI scanning. To achieve maximal safe resection, tumor resection was performed with the guidance of neuronavigation (StealthStation, Medtronic) and 5-aminolevulinic acid fluorescence (5-ALA). After surgery, chemoradiotherapy was performed when patients were stable. Extent of resection was assessed according to the postoperative MRI scans within 72 hours, classified as either gross total resection, subtotal resection or biopsy of the contrast enhanced tumor region. Patients were followed up in our neuro-oncology clinics. Treatment response and tumor progression was evaluated according to the Response Assessment in Neuro-oncology criteria (7). All MRI and histological data were collected prospectively, whereas survival data were analyzed retrospectively to avoid the issue of pseudoprogression. Among the cohort, 31 of 115 (27.0%) patients were previously included in a study which reported the utility of diffusion abnormalities for indication of extent of resection (15); 50 of 115 (43.5%) patients were reported to reveal the diffusion and metabolic change in peritumoral area glioblastoma (16); 64 of 115 (55.7%) patients were reported in another study which identified the correlation between a less invasive phenotype with IDH mutation (17). This current

manuscript reports a novel approach using joint histogram analysis of tensor decomposition to explore the intratumoral heterogeneity of glioblastoma.

Pro-operative MRI acquisition

A 3-Tesla MRI system (Magnetron Trio; Siemens Healthcare, Erlangen, Germany) with a standard 12-channel receive-head coil was used for MRI acquisition. MRI sequences included anatomical and diffusion tensor imaging. The anatomical sequences were acquired as following: post-contrast T1-weighted imaging (TR/TE/TI 2300/2.98/900 ms; flip angle 9°; FOV 256 × 240 mm; 176-208 slices; no slice gap; voxel size 1.0 × 1.0 × 1.0 mm,) after intravenous injection of 9 mL gadobutrol (Gadovist,1.0 mmol/mL; Bayer, Leverkusen, Germany); T2-weighted fluid attenuated inversion recovery (FLAIR) (TR/TE/TI 7840-8420/95/2500 ms; refocusing pulse flip angle 150°; FOV 250 × 200 mm; 27 slices; 1 mm slice gap; voxel size of 0.78 × 0.78 × 4.0 mm). DTI was acquired with a single-shot echo-planar sequence (TR/TE 8300/98 ms; flip angle 90°; FOV 192 × 192 mm; 63 slices; no slice gap; voxel size 2.0 × 2.0 × 2.0 mm; 12 directions; b values: 350, 650, 1000, 1300, and 1600 sec/mm^2; imaging time: 9 minutes 26 seconds).

Imaging processing

For each subject, DTI images were firstly processed with the diffusion toolbox (FDT) (18) of FSL v5.0.8 (FMRIB Software Library, Centre for Functional MRI of the Brain, Oxford, UK) (19). For each voxel of the processed images, the isotropic component (p) and the anisotropic component (q) of DTI were calculated by using the previously described equation (11). Anatomical MRI images were coregistered to the processed

diffusion tensor images with an affine transformation, using the FSL linear image registration tool (FLIRT) (20).

Tumor regions of interest (ROIs) were manually drawn on the post-contrast T1 and FLAIR images using an open-source software 3D slicer v4.6.2 (https://www.slicer.org/) (21) by a neurosurgeon with > 8 years of experience (CL), and a researcher with > 4 years of brain tumor image analysis experience (NRB) and reviewed by a neuroradiologist with > 8 years of experience (TM). Non-enhancing ROI, defined as the non-enhancing region outside of contrast-enhanced region, were obtained in MATLAB (MathWorks, Inc., Natick MA) by Boolean operations on contrast-enhancing and FLAIR tumor ROIs. For each individual subject, normal-appearing white matter was drawn manually in the contralateral white matter as normal controls. Volumetric analysis of all ROIs was performed in FSL by using the function of fslmaths (19). Inter-rater reliability testing was performed using Dice similarity coefficient scores.

Histogram analysis

Both univariate and joint histogram analysis were performed in the Statistics and Machine Learning Toolbox of MATLAB. The contrast-enhancing and non-enhancing ROIs were analyzed independently. A demonstration of histogram analysis was summarized in Figure 1. Firstly, DTI-p and -q values were obtained from the ROI on a voxel-by-voxel basis. Each tumor voxel value was normalized by dividing it by the mean voxel value of the contralateral normal-appearing white matter. Next, the univariate histograms of DTI-p and -q were constructed from the normalized voxel

values using 100 bins within the range 0~5 (Figure 1. A & B). The height of the bins represented the relative frequency of the voxels falling into a specific DTI-p or -q value range. The mean, median, 25th and 75th percentiles of the univariate histogram were calculated.

The joint histogram was constructed with the x- and y-axis representing the normalized DTI-p and -q values respectively, using 50×50 bins within the range of 0~5 on both axes (Fig 1. C). All voxels from the ROI were assigned to the corresponding histogram bins in the 3D space, according to the DTI-p and -q values they carried. The bin height of the joint histogram represented the relative frequency of the voxels simultaneously falling into a specific DTI-p and -q value ranges. Since the DTI-p and -q values of each voxel have been normalized as above mentioned, the coordinator point (p=1, q=1) was designated to represent the mean diffusion pattern in the contralateral normal-appearing white matter. Thus, according to the relative position to the coordinator point (p=1, q=1), four voxel groups describing the co-occurrence distribution of DTI-p and -q abnormality were obtained, (Fig 1. D), namely:

I. Voxel Group I (decreased DTI-p/decreased DTI-q, p↓/q↓)
II. Voxel Group II (decreased DTI-p/increased DTI-q, p↓/q↑)
III. Voxel Group III (increased DTI-p/increased DTI-q, p↑/q↑)
IV. Voxel Group IV (increased DTI-p/decreased DTI-q, p↑/q↓)

The proportion of each voxel group in the ROI (calculated as the summed voxels divided by the total ROI volume) were used as the joint histogram features. These

joint histogram features were obtained from both contrast-enhancing and non-enhancing tumor regions, leading to 8 features for each patient.

Assessment of IDH-1 R132H Mutation and MGMT Methylation Status

IDH-1 R132H mutation was firstly evaluated via immunohistochemistry. After the paraffin was removed and a heat-induced antigen retrieval was performed, IDH-1 R132H mutation-specific antibody (Dianova, Hamburg, Germany) was applied at a 1:20 dilution on slices. A secondary antibody avidin-based detection system was used. In five patients for whom IDH-1 R132H mutation was not detected by immunohistochemistry, tumor DNA was extracted from tumor-rich tissue and sequenced for other rare IDH mutation in codon 132 of the IDH-1 gene and codon 172 of the IDH2 gene using the targeted next generation sequencing (Ion AmpliSeq Cancer Hotspot Panel v2 and (Ion PGM System; Thermo Fisher Scientific).

MGMT promoter methylation status was evaluated as follows: DNA was extracted from the dissected neoplastic cell-rich tissue and was bisulphite-converted using the EpiTect Bisulphite Kit (Qiagen). Pyrosequencing of four CpG sites (CpGs 76-79) in exon 1 of the MGMT gene was then performed by using the CE-Marked therascreen MGMT Pyro Kit on a Pyromark Q24 System (Qiagen). A cut-off of 10% mean methylation for the four CpG sites was used to determine tumors as either methylated or unmethylated based on the published data (22, 23).

Evaluation of tumor progression rate

Tumor progression was diagnosed in our neuro-oncology clinics by the multidisciplinary team. The time to progression was defined as the time period between the surgery date and the date of the first MRI T1W image with contrast that showed tumour progression (as determined by a consultant neuroradiologist). Available tumor progression images were collected by one of the authors (JLY, a neurosurgeon with > 10 years of experience) and reviewed by three authors (CL, JLY and RJP). A two-stage semiautomatic coregistration between the progression images and pre-operative postcontrast T1-weighted images was performed using a previously reported tool (24). This coregistration method firstly calculated the transformation matrix between the pre-operative lesion and tumor cavity on progression images. The matrix was then applied to the brain parenchyma (15). After coregistration, the progression tumor volume was calculated using FSL function of fslmaths. The progression rate was calculated as the progression tumor volume divided by time to progression.

Statistics

All analyses were performed in RStudio v3.2.3 (https://www.rstudio.com/). Two parametric continuous variables were compared with the Welch Two Sample t-test. Two non-parametric variables, i.e., histogram features or tumor volume, were compared with Wilcoxon signed rank test. Cox proportional hazards regression method was performed to evaluate patient survival considering all the confounders, including IDH-1 mutation status, MGMT methylation status, sex, age, extent of resection, contrast-enhancing tumor volume, together with each univariate and joint histogram feature. Patients who were alive at the last known follow-up were

censored. Logistic regression models were used to test prognostic values of covariates for 12-, and 24-month overall survival (OS) and progression-free survival (PFS). All the confounders of IDH-1 mutation status, MGMT methylation status, sex, age, extent of resection, contrast-enhancing tumor volume were included in the baseline models. The histogram features were added one by one into the baseline model to assess their incremental prognostic value. Receiver Operator Characteristics (ROC) curves were generated and the area under the curve (AUC) were compared using one-way ANOVA. For the Kaplan-Meier analysis, the continuous variables were dichotomized using optimal cutoff values, which were calculated by the function of 'surv_cutpoint' in R Package "survminer". Significance was accepted at a two-sided significance level of alpha < 0.05.

Results

Patients and regions of interest

In total, 136 patients were recruited for this study. After surgery, 115 (84.6%) histologically confirmed glioblastoma patients (mean age 59.3 years, range 22 - 76 years, 87 males) were included. Twenty-one patients were excluded due to the non-glioblastoma pathology diagnosis. Among the included 115 patients, 84 (73.0 %) patents received standard dose of radiotherapy plus temozolomide concomitant and adjuvant chemotherapy post-operatively. Survival data were available for 79 (94.0%) of these patients and 5 (6.0%) patients were lost to follow up. IDH-1 mutation status was available for 114 patients and 7 of 114 (6.1%) patients were IDH-1 mutant. In the remaining 107 patients, an IDH-1 R132H or other rare IDH-1 and IDH-2 mutations where screened were not detected. MGMT-methylation status was available for 75 patients, among which 29 (38.7%) patients were methylated. The median OS was 424 days (range 52 -1376 days) and the median PFS was 262 days (range 25-1130 days). Patient clinical characteristics are summarized in Table 1. Inter-rater reliability testing of regions of interest (ROIs) showed excellent agreement between the two raters, with Dice scores (mean ± standard deviation [SD]) of 0.85 ± 0.10 and 0.86 ± 0.10 for contrast-enhancing and non-enhancing ROIs respectively. The volumes (mean ± SD) of contrast-enhancing and non-enhancing ROIs were 53.6 ± 33.8 cm^3 and 62.5 ± 44.0 cm^3 respectively.

Diffusion signatures of contrast-enhancing and non-enhancing regions

The diffusion signatures of contrast-enhancing and non-enhancing regions are demonstrated in Table 2. The comparisons of all histogram features between

contrast-enhancing and non-enhancing regions showed significance (each $p < 0.01$), suggesting the two regions had distinct diffusion patterns. For the univariate features, both contrast-enhancing and non-enhancing regions displayed increased DTI-p (with a value of all >greater than 1), compared to normal-appearing white matter, although the increase in contrast-enhancing region is more significant. A consistently decreased DTI-q (with a value of less than 1) was observed in contrast-enhancing region, whereas non-enhancing region displayed increased mean and 75th percentile in DTI-q. Generally, contrast-enhancing region displayed a more significantly increased DTI-p and decreased DTI-q than non-enhancing region.

In accordance with the univariate features, joint histogram analysis showed that Voxel Group IV (increased DTI-p/decreased DTI-q, p↑/q↓) accounted for the largest proportion in both contrast-enhancing and non-enhancing regions. A significantly higher proportion of Voxel Group IV (p↑/q↓) was found in contrast-enhancing region than non-enhancing region ($p < 0.001$). By contrast, non-enhancing region displayed significantly higher proportion of Voxel Group II (p↓/q↑) and Voxel Group III (p↑/q↑) (both $p < 0.001$) than contrast-enhancing region.

Multivariate survival analysis

The multivariate survival modeling of PFS and OS were tested in 56 patients for whom all confounders including IDH-1 mutation, MGMT methylation status and histogram features were available. The results of the multivariate Cox-regression analysis were shown in Table 3.

Four of 8 joint histogram features significantly contributed to both OS and PFS. Specifically, higher proportion of Voxel Group IV (p↑/q↓) in contrast-enhancing region contributed to a better PFS and OS (both HR = 0.97, CI: 0.95- 0.99, *p* = 0.003). Similar contribution to PFS and OS was observed from Voxel Group IV (p↑/q↓) in non-enhancing region (both HR = 0.97, CI: 0.95- 0.99, *p* = 0.001). By contrast, higher proportion of two voxel groups in non-enhancing region contributed to worse survival: Voxel Group II (p↓/q↑) (for PFS: HR = 1.12, CI: 1.06-1.18, *p* < 0.001; for OS: HR = 1.12, CI: 1.07-1.18, *p* < 0.001); and Voxel Group III (p↑/q↑) (for PFS: HR = 1.03, CI: 1.01-1.05, *p* = 0.009; for OS: HR = 1.03, CI: 1.003-1.05, *p* = 0.022). The survival curves using Kaplan-Meier method were demonstrated in Figure 2, with *p* values from Log-rank test.

Incremental prognostic value of joint histogram features

The results of model comparisons were shown in Table 4. For the prediction of 12-month PFS and OS, the AUC of the baseline multivariate models (including IDH-1 mutation, MGMT methylation status and other clinical factors) were 0.80 (0.69-0.91) and 0.73 (0.59-0.87) respectively. For the prediction of 24-month PFS and OS, the AUC of the baseline multivariate models were 0.81 (0.69-0.92) and 0.71 (0.57-0.84) respectively. The incremental prognostic value of joint histogram features was assessed by adding them into the baseline models successively. Significantly increased diagnostic accuracy (each *p* < 0.05) was observed from 3 joint histogram features in non-enhancing region: Voxel group II (p↓/q↑), Voxel group III (p↑/q↑) and Voxel group IV (p↑/q↓).

Correlations with tumor progression rate and FLAIR volume

Further, we performed correlation tests in above 3 of 8 joint histogram features which showed significantly incremental diagnostic accuracy. First, the correlation with tumor progression rate was tested in 57 patients had progression and with available MR images at progression. The progression volume (mean ± SD) was 14.32 ± 21.97 cm^3. The progression rate (mean ± SD) was 0.003 ± 0.013 cm^3/day. The results showed that Voxel Group II (p↓/q↑) in non-enhancing region had a significant positive correlation (p = 0.010, r = 0.35) with the progression rate, whereas Voxel Group IV (p↑/q↓) in non-enhancing region (p = 0.040, r = -0.28) showed a negative correlation. No significant correlations were found Voxel Group III (p↑/q) in non-enhancing region.

We then analyzed the correlations between the tumor infiltrated volume on FLAIR and the proportions of voxel groups. The results showed that the proportion of Voxel Group II (p↓/q↑) in non-enhancing region showed a significant negative correlation (p < 0.001, r = -0.57) with FLAIR volume, whereas the proportion of Voxel Group IV (p↑/q↓) in non-enhancing region (p < 0.001, r = 0.37) showed positive correlation. No significant correlation was found with the proportion of Voxel Group III (p↑/q↑) in non-enhancing region. The above correlations were shown in Figure 3. Two examples of pre-operative and progression images, as well as the annotated subregions of Voxel Group II and Voxel Group III in non-enhancing region are demonstrated in Figures 4 & 5.

Discussion

In this study, we found that preoperative joint histogram analysis using DTI-p and -q can reflect the heterogeneity of tumor infiltration. The histogram features obtained with this method can improve the prognostic value of IDH-1 mutation and MGMT promoter methylation status, and be useful in detection of tumor subregion which might be responsible for progression.

Previous studies have shown that DTI has potential in studying tumor infiltration (25). However, the interpretation of tensor data is challenging, due to the high dimensionality. Substantial efforts have been made to simplify the tensor data into scalar measures. Among these markers, fractional anisotropy (FA) and mean diffusivity (MD) are most commonly used (11). However, since FA can be affected by both the anisotropic and isotropic components (according to its definition equation), its utility is not consistent in detecting tumor infiltration. An enhanced visualization and quantification of tensor imaging was subsequently advanced by decomposing the raw tensor into isotropic (p) and anisotropic (q) components (7). This technique has shown its utility in detecting the subtle change caused by tumor invasion and predicting progression (17). Consistent with previous studies, our results showed an increased DTI-p and decreased DTI-q in most univariate histogram features, which have been previously shown to be biomarkers of bulk tumour and invasive tumour. However, our results also suggested non-enhancing tumor region may display increased mean and 75th percentile of DTI-q.

One single marker is insufficient to reflect the full tensor. Moreover, it is suggested to combine DTI measures with structural imaging modalities (26). To achieve this, we proposed the current joint histogram analysis of DTI-p and -q within the tumor regions identified on anatomical sequences. The results showed the Voxel Group IV (p↑/q↓) had the largest proportion. In this subregion, the brain microstructure was displaced to allow more isotropic movement of water molecules. The displacement of fibers also means the 'fast track' to infiltrate was diminishing and thus lead to the decreased anisotropic movement. The significantly higher proportion of this diffusion pattern in the bulk tumor than the infiltrated tumor may suggest more substantial fiber damage within the bulk tumor.

More diffusion patterns can be revealed by this approach. Particularly, the higher proportions of Voxel Group II (p↓/q↑) and Voxel Group III (p↑/q↑) in the non-enhancing region may suggest a less disrupted white matter tract. In these regions, water molecules tend to behave higher anisotropic movement. Since the decreased DTI-p is thought to reflect the elevated cell density, the tumor subregion identified by Voxel Group II (p↓/q↑) in non-enhancing region, may represent a migratory tumor habitat with higher cellularity. Though the proportion is relatively low, the contribution to patient survival and tumor progression rate indicated its higher invasiveness and should be treated with more attention in surgical planning. As shown in the case example, the location of this subregion is in the vicinity of surgical cavity, an extended resection might be considered for these subregions. Histological correlation of these findings is required.

The joint histogram features found in our study showed clinical significance, with incremental prognostic values when integrated over clinical factors. As the more invasive subregion identified, targeted tumor resection and radiation therapy can perhaps be achieved, which may reduce the radiation damage to the normal brain and enhance the efficacy of treatment. Also, this proposed approach may be applied to a broader imaging research field to meet the demand of multiple modality imaging analysis.

There are some limitations in our study. Firstly, the patient population reported is from a single center and the results were not validated by another cohort. Secondly, although our current study did not have biological validation, previous studies have validated the histological correlates of DTI-p and DTI-q by image-guided biopsies (8). This current study presented more comprehensive measure of tumor infiltration with the joint analysis of these two directional components.

In conclusion, we used a novel approach of joint histogram analysis of DTI-p and -q to study the intratumoral heterogeneity of tumor invasion. The results showed that this approach may help to better understand tumor infiltration. In non-enhancing region, decreased DTI-p and increased DTI-q may be able to define an invasive subregion responsible for tumor progression. This finding may be useful in targeted surgery and radiation therapy.

Table 1. Clinical characteristics

Variable	Patient Number
Age at diagnosis	
<60	40
≥60	75
Sex	
Male	87
Female	28
Extent of resection (of enhancing tumor)	
Complete resection	77
Partial resection	32
Biopsy	6
MGMT-methylation status*	
Methylated	29
Unmethylated	46
IDH-1 mutation status	
Mutant	7
Wild-type	107
Tumor volumes(cm^3) #	
Contrast-enhancing	53.6 ± 33.8
Non-enhancing	62.5 ± 44.0
Survival (days)	
Median OS (range)	424 (52 -1376)
Median PFS (range)	262 (25-1130)

*MGMT-methylation status unavailable for 40 patients; #mean ± SD of original data. SD: standard deviation; MGMT: O-6-methylguanine-DNA methyltransferase; IDH-1: Isocitrate dehydrogenase 1; cm: centimeters; OS: overall survival; PFS: progression-free survival.

Table 2. Histogram measures

Variable	contrast-enhanced region	non-enhancing region	*p* value
	Mean ± SD	Mean ± SD	
DTI-p histogram features			
25th percentile	1.18 ± 0.23	1.11 ± 0.15	**< 0.001**
Median	1.47 ± 0.38	1.32 ± 0.23	**0.001**
Mean	1.57 ± 0.36	1.37 ± 0.22	**< 0.001**
75th percentile	1.90 ± 0.60	1.59 ± 0.30	**< 0.001**
DTI-q histogram features			
25th percentile	0.42 ± 0.14	0.71± 0.18	**< 0.001**
Median	0.65 ± 0.19	0.95 ± 0.23	**< 0.001**
Mean	0.71 ± 0.19	1.01 ± 0.24	**< 0.001**
75th percentile	0.93 ± 0.24	1.24 ± 0.29	**< 0.001**
DTI Joint histogram features (%)			
Voxel Group I	8.49 ± 10.37	5.49 ± 6.17	**< 0.001**
Voxel Group II	3.82 ± 4.92	7.27 ± 8.07	**< 0.001**
Voxel Group III	20.78 ± 13.65	40.33 ± 18.97	**< 0.001**
Voxel Group IV	66.90 ± 16.28	46.92 ± 20.40	**< 0.001**

DTI: diffusion tensor imaging; SD: standard deviation; Voxel Group I: decreased DTI-p, decreased DTI-q (p↓/q↓,); Voxel Group II: decreased DTI-p, increased DTI-q (p↓/q↑); Voxel Group III: increased DTI-p, increased DTI-q (p↑/q↑); Voxel Group IV: increased DTI-p, decreased DTI-q (p↑/q↓).

Table 3. Cox multivariate modeling of survivals

Variable	Progression-free survival*			Overall survival*		
	HR	95%CI	*p* value	HR	95%CI	*p* value
contrast-enhancing region						
Voxel Group I	1.02	0.98-1.06	0.335	1.05	1.01-1.09	**0.014**
Voxel Group II	1.06	0.998-1.14	0.058	1.08	1.02-1.16	**0.015**
Voxel Group III	1.03	1.01-1.06	**0.010**	1.02	0.997-1.05	0.086
Voxel Group IV	0.97	0.95- 0.99	**0.003**	0.97	0.95- 0.99	**0.003**
non-enhancing region						
Voxel Group I	0.99	0.88-1.12	0.918	1.08	0.97-1.21	0.159
Voxel Group II	1.12	1.06-1.18	**< 0.001**	1.12	1.07-1.18	**< 0.001**
Voxel Group III	1.03	1.01-1.05	**0.009**	1.03	1.003-1.05	**0.022**
Voxel Group IV	0.97	0.95-0.99	**0.001**	0.97	0.95-0.99	**0.001**

*Cox models accounted for IDH-1 mutation status, MGMT methylation status, sex, age, extent of resection and contrast-enhancing tumor volume. HR: hazard ratio; CI: confidence interval; DTI: diffusion tensor imaging; Voxel Group I: decreased DTI-p, decreased DTI-q (p↓/q↓,); Voxel Group II: decreased DTI-p, increased DTI-q (p↓/q↑); Voxel Group III: increased DTI-p, increased DTI-q (p↑/q↑); Voxel Group IV: increased DTI-p, decreased DTI-q (p↑/q↓).

Table 4. Model Comparison

Model	12 month AUC	95% CI	*p* value	24 month AUC	95% CI	*p* value
Progression-free survival						
baseline*	0.80	0.69-0.91		0.81	0.69-0.92	
Contrast-enhancing region						
+Voxel Group I	0.82	0.72-0.93	0.050	0.80	0.68-0.92	0.765
+Voxel Group II	0.79	0.67-0.90	0.730	0.81	0.69-0.93	0.475
+Voxel Group III	0.80	0.69-0.91	0.400	0.81	0.70-0.93	0.088
+Voxel Group IV	0.81	0.71-0.92	0.100	0.82	0.70-0.93	0.074
Non-enhancing region						
+Voxel Group I	0.79	0.67-0.91	0.875	0.81	0.69-0.92	0.483
+Voxel Group II	0.85	0.75-0.94	**0.004**	0.82	0.71-0.94	0.102
+Voxel Group III	0.81	0.70-0.92	0.085	0.87	0.76-0.97	**0.002**
+Voxel Group IV	0.84	0.74-0.94	**0.009**	0.87	0.76-0.97	**0.002**
Overall survival						
baseline*	0.73	0.59-0.87		0.71	0.57-0.84	
Contrast-enhancing region						
+Voxel Group I	0.75	0.61-0.89	0.078	0.70	0.56-0.84	0.574
+Voxel Group II	0.74	0.60-0.88	0.389	0.70	0.56-0.84	0.771
+Voxel Group III	0.73	0.59-0.87	0.940	0.72	0.59-0.85	0.122
+Voxel Group IV	0.76	0.62-0.90	0.207	0.71	0.58-0.84	0.107
Non-enhancing region						
+Voxel Group I	0.73	0.60-0.87	0.710	0.72	0.58-0.85	0.734
+Voxel Group II	0.76	0.62-0.90	0.094	0.73	0.60-0.86	0.253
+Voxel Group III	0.76	0.64-0.89	0.070	0.77	0.65-0.89	**0.011**
+Voxel Group IV	0.79	0.67-0.91	**0.026**	0.77	0.65-0.89	**0.012**

*Baseline model was built with IDH-1 mutation status, MGMT methylation status, sex, age, extent of resection and contrast-enhancing tumor volume. AUC: area under receiver operator characteristics curve; HR: hazard ratio; CI: confidence interval; DTI: diffusion tensor imaging; Voxel Group I: decreased DTI-p, decreased DTI-q (p↓/q↓,); Voxel Group II: decreased DTI-p, increased DTI-q (p↓/q↑); Voxel Group III: increased DTI-p, increased DTI-q (p↑/q↑); Voxel Group IV: increased DTI-p, decreased DTI-q (p↑/q↓).

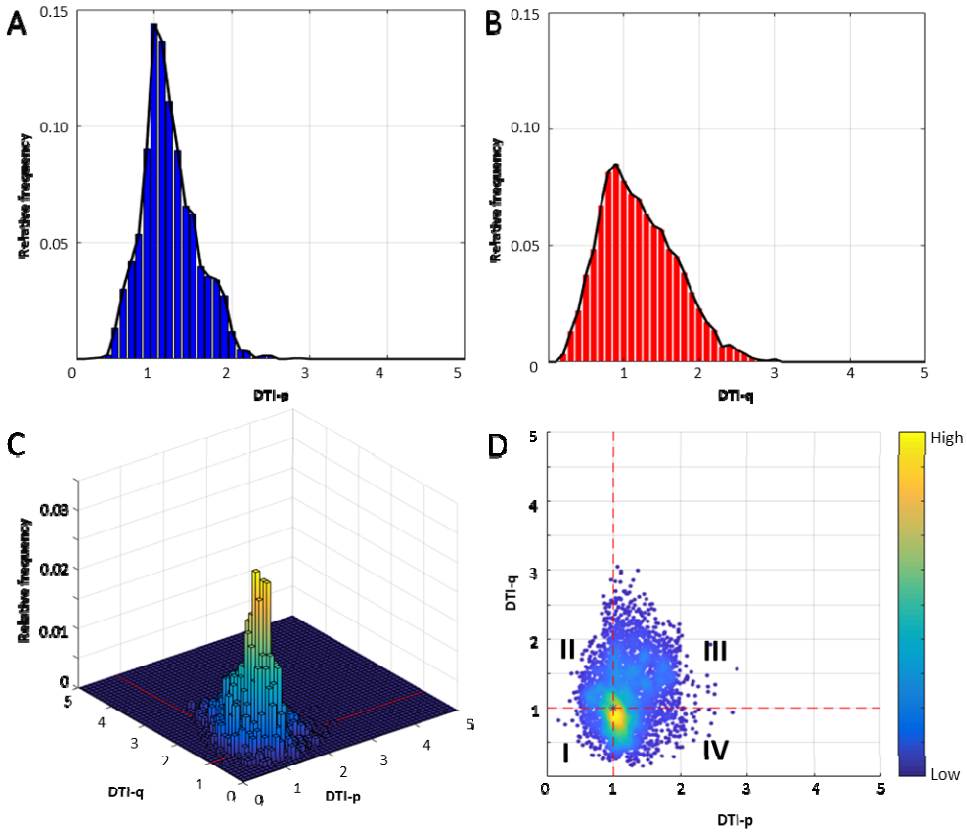

Figure 1. Illustration of the univariate and joint histogram analysis. Univariate histograms of DTI-p (A) and -q (B) were generated using 100 bins. The joint histogram was generated with x- and y-axis representing DTI-p and -q values using 50 × 50 bins. The bin height of the joint histogram represented the relative frequency of voxels in the ROI falling into a specific DTI-p and -q range (C). Four voxel groups of DTI-p and -q abnormalities were obtained (D): I. Voxel Group I (decreased DTI-p/decreased DTI-q); II. Voxel Group II (decreased DTI-p/increased DTI-q); III. Voxel Group III (increased DTI-p/increased DTI-q); IV. Voxel Group IV (increased DTI-p/decreased DTI-q).

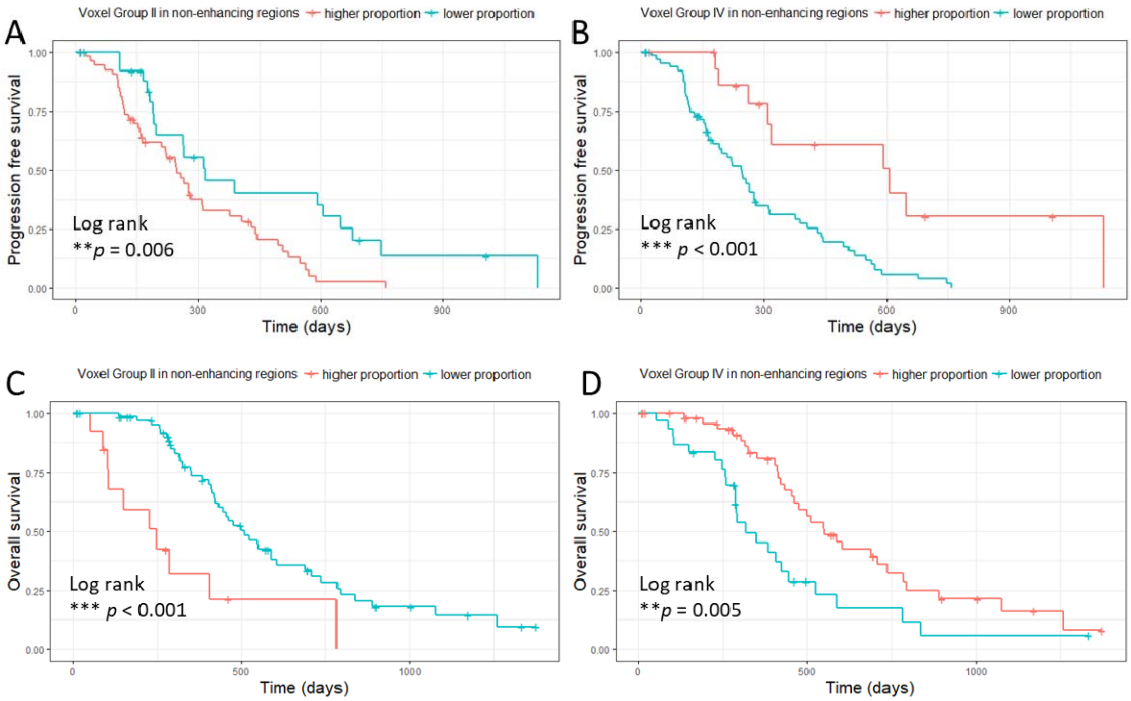

Figure 2. Kaplan-Meier plots of survival analysis. Log-rank test showed lower proportion of Voxel Group II in non-enhancing tumor region was associated with better PFS ($p = 0.006$) (A) and better OS ($p < 0.001$) (C). Higher proportion of Voxel Group IV in non-enhancing tumor region was associated with better PFS ($p < 0.001$) (B) and better OS ($p = 0.005$) (D).

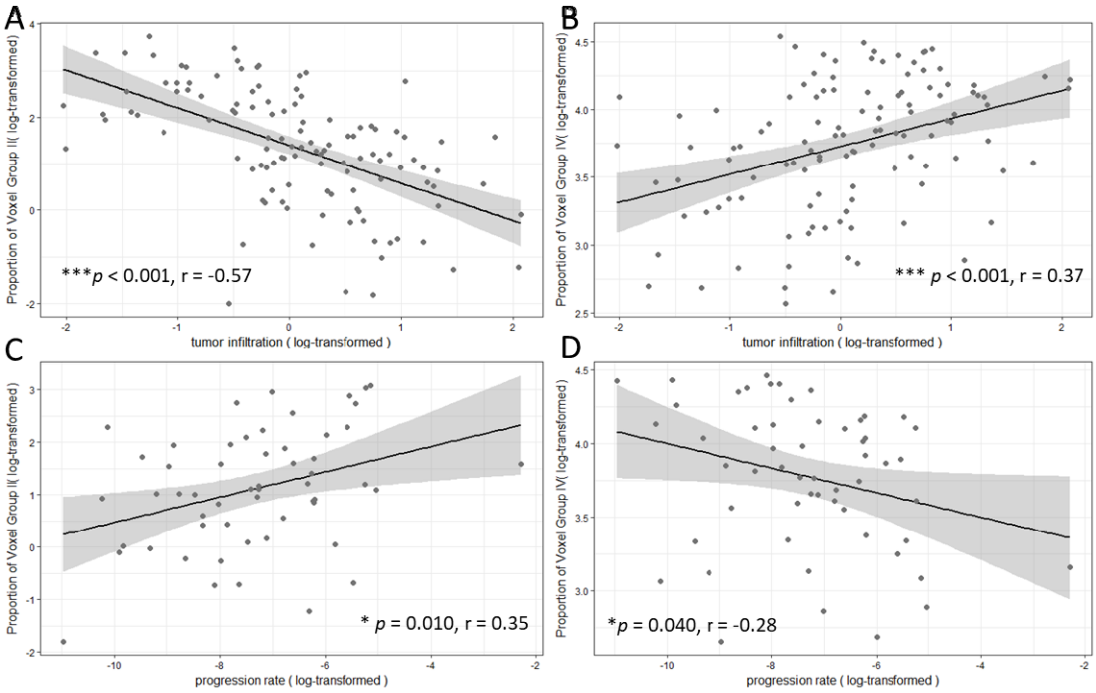

Figure 3. The correlations between the proportions of pixel groups in non-enhancing region with tumor progression rate/infiltration area. Voxel Group II in non-enhancing region showed a significant negative correlation with tumor infiltration area shown on FLAIR images (normalized by contrast-enhancing volume) (A) and a positive correlation with the progression rate (C), whereas Voxel Group IV in non-enhancing region showed a positive correlation with tumor infiltration area shown on FLAIR images (normalized by contrast-enhancing volume) (B) and with the progression rate (D).

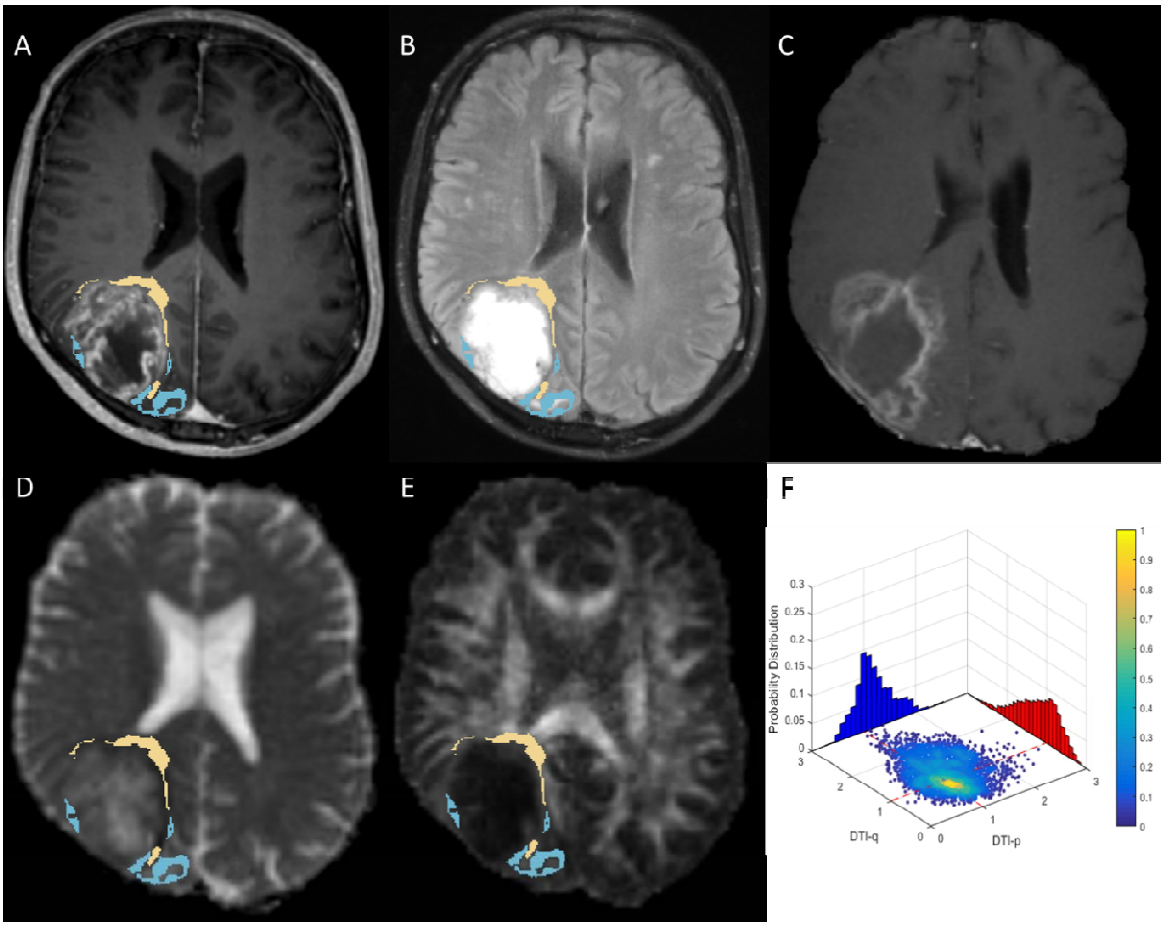

Figure 4. The Voxel Group II (yellow) and Voxel Group IV (blue) of non-enhancing in a case 1. The 63-year-old man was radiologically diagnosed with primary glioblastoma (A & B). Volumetric analysis of pre-operative MRI showed contrast enhanced tumor volume was 83.57 cm^3. The patient received tumor resection with the guidance of neuronavigation and 5-aminolevulinic acid fluorescence with the aim of maximal resection, but only subtotal resection was achieved according to 72h post-operative MRI. Pathological assessment confirmed this was a MGMT-methylated glioblastoma and IDH mutation was negative. The patient received concomitant and adjuvant temozolomide chemoradiotherapy. The progression-free survival of this patient was 47 days and overall survival was 104 days. The post-contrast T1-weighted imaging showed the progression was around the resection cavity (C). The joint histogram analysis of pre-operative DTI-p (D) and DTI-q (E) maps showed Voxel Group II occupied 15.54% in the non-enhancing tumor and Voxel Group IV occupied 28.24 % of the non-enhancing tumor (F). The subregion of Voxel Group II in the non-enhancing tumor (yellow) corresponded to the progression location.

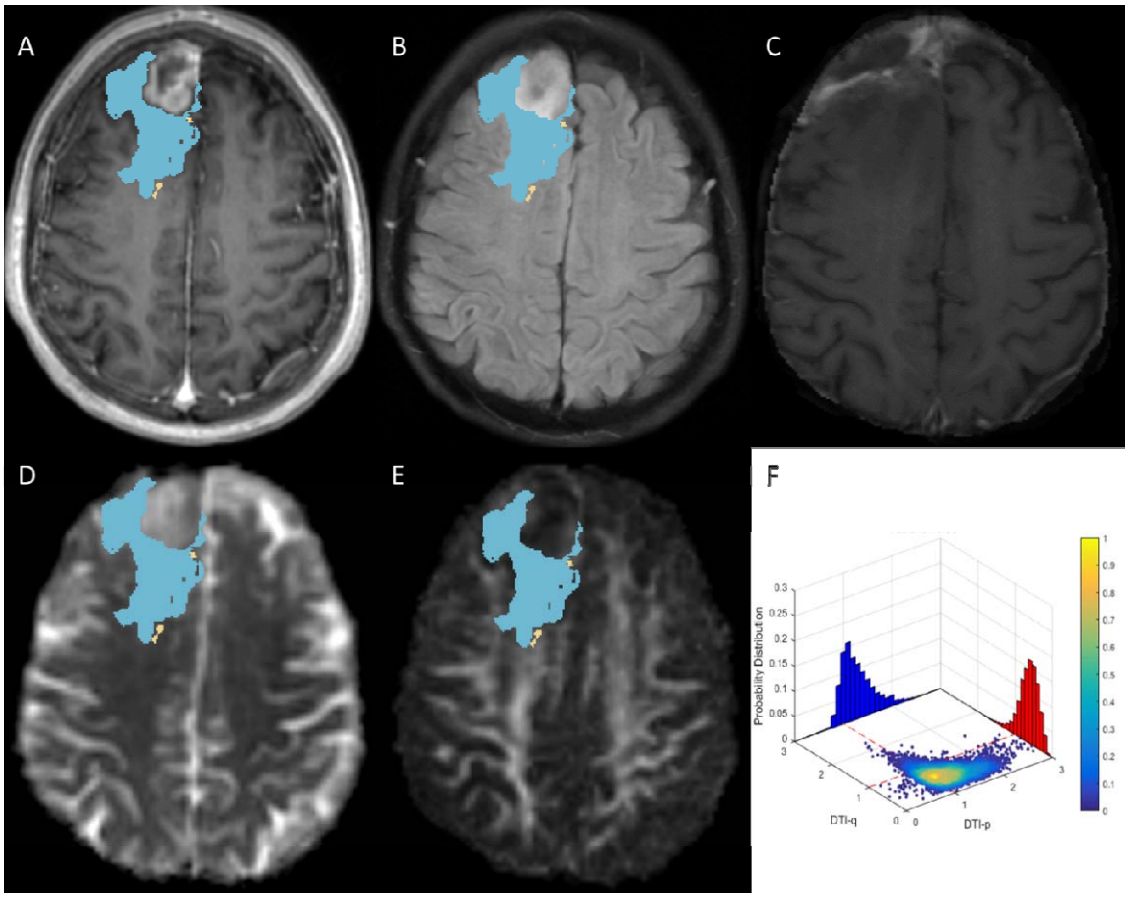

Figure 5. The Voxel Group II (yellow) and Voxel Group IV (blue) of non-enhancing in a case 2. The 65-year-old man was radiologically diagnosed with primary glioblastoma (A & B). Volumetric analysis showed contrast enhanced tumor volume was 37.39 cm^3. Gross total resection was achieved in this patient with the guidance of neuronavigation and 5-aminolevulinic acid fluorescence. Pathological assessment confirmed a MGMT-methylated glioblastoma and IDH mutation was negative. The patient received concomitant and adjuvant temozolomide chemoradiotherapy. The progression-free survival of this patient was 1006 days and was alive in the last follow-up. Post-contrast T1-weighted imaging showed a minor progression around the resection cavity (C). The joint histogram analysis of pre-operative DTI-p (D) and DTI-q (E) maps showed Voxel Group II occupied 2.29 % of the non-enhancing tumor and Voxel Group IV occupied 81.45 % of the non-enhancing tumor (F).

1. Ricard D, Idbaih A, Ducray F, Lahutte M, Hoang-Xuan K, Delattre JY. Primary brain tumours in adults. Lancet. 2012;379(9830):1984-96.
2. Weller M, van den Bent M, Tonn JC, Stupp R, Preusser M, Cohen-Jonathan-Moyal E, et al. European Association for Neuro-Oncology (EANO) guideline on the diagnosis and treatment of adult astrocytic and oligodendroglial gliomas. Lancet Oncol. 2017.
3. Giese A, Bjerkvig R, Berens ME, Westphal M. Cost of migration: Invasion of malignant gliomas and implications for treatment. J Clin Oncol. 2003;21(8):1624-36.
4. Price SJ, Jena R, Burnet NG, Carpenter TA, Pickard JD, Gillard JH. Predicting patterns of glioma recurrence using diffusion tensor imaging. Eur Radiol. 2007;17(7):1675-84.
5. Sottoriva A, Spiteri I, Piccirillo SG, Touloumis A, Collins VP, Marioni JC, et al. Intratumor heterogeneity in human glioblastoma reflects cancer evolutionary dynamics. Proc Natl Acad Sci U S A. 2013;110(10):4009-14.
6. Verhaak RG, Hoadley KA, Purdom E, Wang V, Qi Y, Wilkerson MD, et al. Integrated genomic analysis identifies clinically relevant subtypes of glioblastoma characterized by abnormalities in PDGFRA, IDH1, EGFR, and NF1. Cancer Cell. 2010;17(1):98-110.
7. Wen PY, Macdonald DR, Reardon DA, Cloughesy TF, Sorensen AG, Galanis E, et al. Updated response assessment criteria for high-grade gliomas: response assessment in neuro-oncology working group. J Clin Oncol. 2010;28(11):1963-72.
8. Price SJ, Jena R, Burnet NG, Hutchinson PJ, Dean AF, Pena A, et al. Improved delineation of glioma margins and comp of infiltration with the use of diffusion tensor imaging: An image-guided biopsy study. Am J Neuroradiol. 2006;27(9):1969-74.
9. Wright K, Abounader R, Bhat K, Viapiano MS, Pope W. Less-Invasive Phenotype Found in IDHmutated than in IDH-WT Glioblastomas: A Diffusion-Tensor Imaging Study. Neuro-Oncology. 2017;19(3):311-.
10. Hambardzumyan D, Bergers G. Glioblastoma: Defining Tumor Niches. Trends Cancer. 2015;1(4):252-65.
11. Pena A, Green HAL, Carpenter TA, Price SJ, Pickard JD, Gillard JH. Enhanced visualization and quantification of magnetic resonance diffusion tensor imaging using the p : q tensor decomposition. Brit J Radiol. 2006;79(938):101-9.
12. Mohsen LA, Shi V, Jena R, Gillard JH, Price SJ. Diffusion tensor invasive phenotypes can predict progression-free survival in glioblastomas. Brit J Neurosurg. 2013;27(4):436-41.
13. Parsons DW, Jones S, Zhang X, Lin JC, Leary RJ, Angenendt P, et al. An integrated genomic analysis of human glioblastoma multiforme. Science. 2008;321(5897):1807-12.
14. Hegi ME, Diserens AC, Gorlia T, Hamou MF, de Tribolet N, Weller M, et al. MGMT gene silencing and benefit from temozolomide in glioblastoma. N Engl J Med. 2005;352(10):997-1003.
15. Yan JL, van der Hoorn A, Larkin TJ, Boonzaier NR, Matys T, Price SJ. Extent of resection of peritumoral diffusion tensor imaging-detected abnormality as a predictor of survival in adult glioblastoma patients. J Neurosurg. 2017;126(1):234-41.
16. Price SJ, Young AMH, Scotton WJ, Ching J, Mohsen LA, Boonzaier NR, et al. Multimodal MRI Can Identify Perfusion and Metabolic Changes in the Invasive Margin of Glioblastomas. J Magn Reson Imaging. 2016;43(2):487-94.
17. Price SJ, Allinson K, Liu H, Boonzaier NR, Yan JL, Lupson VC, et al. Less Invasive Phenotype Found in Isocitrate Dehydrogenase-mutated Glioblastomas than in Isocitrate Dehydrogenase Wild-Type Glioblastomas: A Diffusion-Tensor Imaging Study. Radiology. 2017;283(1):215-21.

18. Behrens TEJ, Woolrich MW, Jenkinson M, Johansen-Berg H, Nunes RG, Clare S, et al. Characterization and propagation of uncertainty in diffusion-weighted MR imaging. Magnet Reson Med. 2003;50(5):1077-88.
19. Smith SM, Jenkinson M, Woolrich MW, Beckmann CF, Behrens TEJ, Johansen-Berg H, et al. Advances in functional and structural MR image analysis and implementation as FSL. Neuroimage. 2004;23:S208-S19.
20. Jenkinson M, Bannister P, Brady M, Smith S. Improved optimization for the robust and accurate linear registration and motion correction of brain images. Neuroimage. 2002;17(2):825-41.
21. Fedorov A, Beichel R, Kalpathy-Cramer J, Finet J, Fillion-Robin JC, Pujol S, et al. 3D Slicer as an image computing platform for the Quantitative Imaging Network. Magn Reson Imaging. 2012;30(9):1323-41.
22. Dunn J, Baborie A, Alam F, Joyce K, Moxham M, Sibson R, et al. Extent of MGMT promoter methylation correlates with outcome in glioblastomas given temozolomide and radiotherapy. Br J Cancer. 2009;101(1):124-31.
23. Collins VP, Ichimura K, Di Y, Pearson D, Chan R, Thompson LC, et al. Prognostic and predictive markers in recurrent high grade glioma; results from the BR12 randomised trial. Acta Neuropathol Commun. 2014;2:68.
24. van der Hoorn A, Yan JL, Larkin TJ, Boonzaier NR, Matys T, Price SJ. Validation of a semi-automatic co-registration of MRI scans in patients with brain tumors during treatment follow-up. Nmr Biomed. 2016;29(7):882-9.
25. Diffusion-Weighted Magnetic Resonance Imaging as a Cancer Biomarker: Consensus and Recommendations. Neoplasia. 2009;11(2):102-25.
26. Bammer R. Basic principles of diffusion-weighted imaging. Eur J Radiol. 2003;45(3):169-84.